J. Fluid Mech. (1979), *vol.* 92, *part* 4, *pp.* 609–629
Printed in Great Britain

Convective instabilities in a closed vertical cylinder heated from below. Part 1. Monocomponent gases

By J. M. OLSON† AND F. ROSENBERGER
Department of Physics, University of Utah, Salt Lake City, Utah 84112

(Received 19 August 1977 and in revised form 8 December 1978)

Kr, Xe and $SiCl_4$ have been investigated for convective instabilities in closed vertical cylinders with conductive walls heated from below. Critical Rayleigh numbers N_{Ra}^{i} for the onset of various convective modes (including the onset of marginally stable and periodic flow) have been determined with a high resolution differential temperature sensing method. Flow patterns were deduced from a multiple sensor arrangement. For the three lowest modes ($i = 1, 2, 3$) good quantitative agreement with linear stability theory is found. Stable oscillatory modes (periodic fluctuations of the mean flow) with a period of approximately 5 s are found for a relatively narrow range of N_{Ra}. The critical Rayleigh number N_{Ra}^{osc} for the onset of oscillatory temperature fluctuations is 1348 ± 50 for an aspect ratio (height/radius) of 6.

1. Introduction

Over the past seventy-five years, a tremendous amount of knowledge has been accumulated about convective instabilities in a semi-infinite, horizontal fluid layer heated from below, i.e. the Rayleigh–Bénard problem. Large regions of parameter space for this problem have been explored and, at this point, are reasonably well characterized [see Koschmieder (1974) and Whitehead (1975) for reviews of this subject]. The picture for other convection geometries is not nearly so complete. In particular, relatively little is known, either experimentally or theoretically, about convective instabilities in a long, vertical column of fluid heated from below. A much broader understanding of convection in this geometry would be especially useful to researchers in the field of crystal growth, where convection in the nutrient phase profoundly affects the growth behaviour of the single crystal. In an effort to improve this situation, we have conducted a series of high resolution experiments designed to study the time-independent and time-dependent convective behaviour of such a system. Specifically, we are concerned in this paper with the stability of monocomponent fluids (gases), contained within a vertical, cylindrically symmetric cell with fixed aspect ratio (height/radius = 6/1) and thermally conducting walls (copper). New results for the steady and the time-dependent convective behaviour will be discussed. A corresponding treatment of some binary fluid systems is presented in a consecutive paper (Olson & Rosenberger 1979).

† Present address: Solar Energy Research Institute, Golden, CO 80401.

0022-1120/79/4242-6750 $02.00

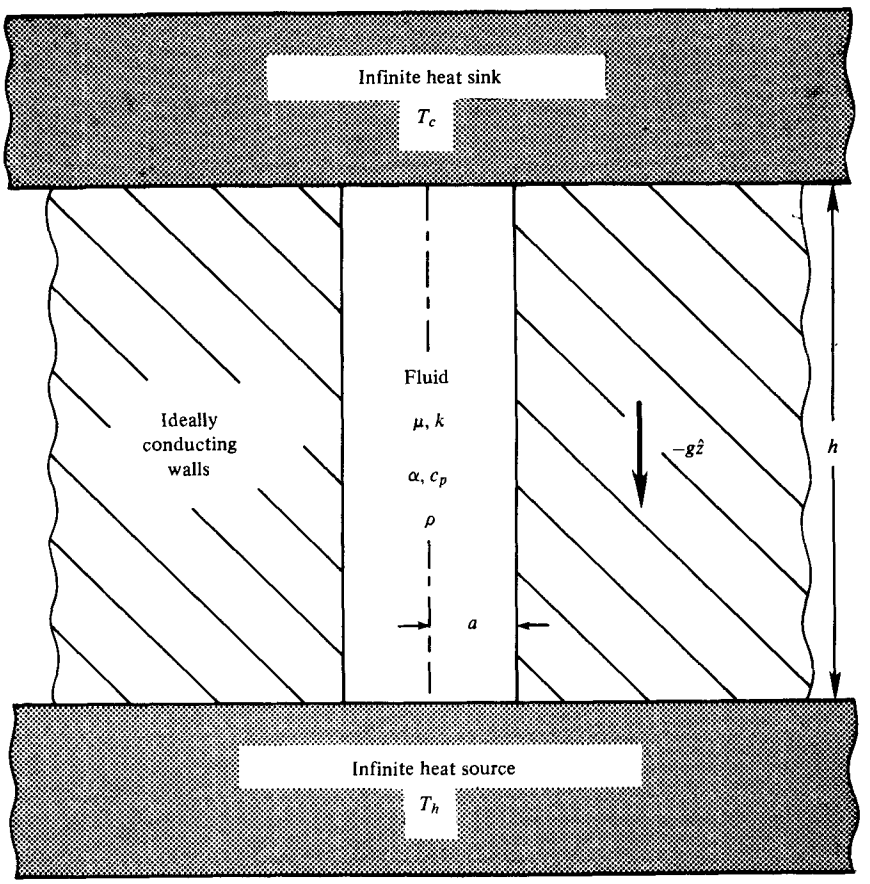

FIGURE 1. Idealized convection geometry.

1.1. *Background*

The idealized system with which we are concerned is shown in figure 1. It consists of a vertical, cylindrical cavity embedded in a material of large thermal conductivity, large relative to the confined fluid. Heat sources and sinks are arranged so that a constant, vertical temperature gradient is imposed across this cell and constant, uniform temperatures, T_c and T_h, are maintained at the top and the bottom of the cell, respectively.

Three dimensionless numbers characterize the hydrodynamic state of the fluid inside the cavity. These are:

(1) the Rayleigh Number, $N_{Ra} = (g\alpha\rho^2 c_p/\mu k) \times (\Delta T a^4/h)$;

(2) the Aspect Ratio, $A = h/a$; and

(3) the Prandtl Number, $N_{Pr} = \mu c_p/k$;

where $\Delta T = T_h - T_c$, h is the height and a is the radius of the cylinder; note the use of a^4/h in N_{Ra} instead of the usual h^3. The mass density ρ, the thermal conductivity k, the dynamic viscosity μ, the specific heat c_p, and α the coefficient of volume expansion are all evaluated at the mean temperature T_m of the fluid.

The original, theoretical work for this problem was done by Hales (1937). He con-

i	1	2	3	4	5	6	7	8
$N_{Ra}^{i}\,(n=1)$	230	280	382	571	898	1437	2266	3457

TABLE 1. Critical Rayleigh number for the onset of the ith asymmetric mode, for a cell with ideally conducting walls and an aspect ratio of 6 (after Catton 1966). Compare with: $N_{Ra}^{1,0} = 475$ (Hales 1937).

sidered the stability of a vertical column of fluid confined by perfectly conducting walls. The ends of the tube were assumed to be idealized, stress-free boundaries. Using a linear perturbation technique, Hales found that there exists a series of eigenvalues ($N_{Ra}^{i,n}$) which determine the onset of the associated 'normal' modes. More recently, other authors have refined and extended the work of Hales. In particular, Yih (1959) has proven the principle of exchange of stabilities for a vertical column of fluid heated from below; hence, the marginally stable state is time-independent. Catton (1966) has calculated $N_{Ra}^{i,n}$ and the associated contributions to the heat flux for the first ten ($i = 1, 2, 3, \ldots, 10$) asymmetric ($n = 1$) modes (see table 1). Yet, he neglected the contribution of the first axisymmetric mode. Charlson & Sani (1971) extended the linear analysis to large n (with $i = 1$).

The critical Rayleigh number for the onset of marginally stable flow is given by the smallest $N_{Ra}^{i,n}$. For large aspect ratios $A \gtrsim \frac{5}{3}$, the smallest $N_{Ra}^{i,n}$ is $N_{Ra}^{1,1}$ (Charlson & Sani 1971). This is equivalent to saying that the planform of the initial instability is a unicellular ($i = 1$), asymmetric ($n = 1$) roll, with flow up one side of the cylinder and down the opposite side (as shown in figure 3*a*). The magnitude of $N_{Ra}^{i,n}$ increases rapidly with n (Charlson & Sani 1971), hence only $N_{Ra}^{i,0}$ and $N_{Ra}^{i,1}$, obtained from linear analysis, have any physical significance. Therefore, in the following the superscript n will be dropped and its value will be specified by use of the terms asymmetric ($n = 1$) and axisymmetric ($n = 0$). Note that in this notation $N_{Ra}^{1} \equiv N_{Ra}^{cr}$.

2. Experimental apparatus and procedure

2.1. *Basic convection cell*

The idealized convection cavity of figure 1 is approximated by the thick-walled copper cell shown in figure 2. The inner surface of the cell is machined and polished to a radius of 1·000 cm. Copper plugs of the appropriate thickness and diameter are press fitted into the ends of the cylinder so that the height of the cavity is 6·00 cm. Six small 'Cajon-type' o-ring feedthroughs arranged in a vertical plane allow for variation of the immersion depth (0–4 mm) of the measurement probes (see §2·2). As the detailed insert of figure 2 shows, the $\frac{1}{16}$ in. bore of each feedthrough ends 1 mm short of the inner wall; the remainder is counter-bored to a diameter of 0·6 mm. Hence, the $\frac{1}{16}$ in. ceramic tube, used to support the small sensors, does not extend into the cavity.

The top of this cell is securely bolted to the top plate of a much larger concentric container. The region between the cell and this external container is continuously evacuated to a pressure of approximately 10^{-2} torr.

The temperature T_c at the top of the cell is established by a water bath which also surrounds the external container. The temperature T_h at the bottom of the cell is

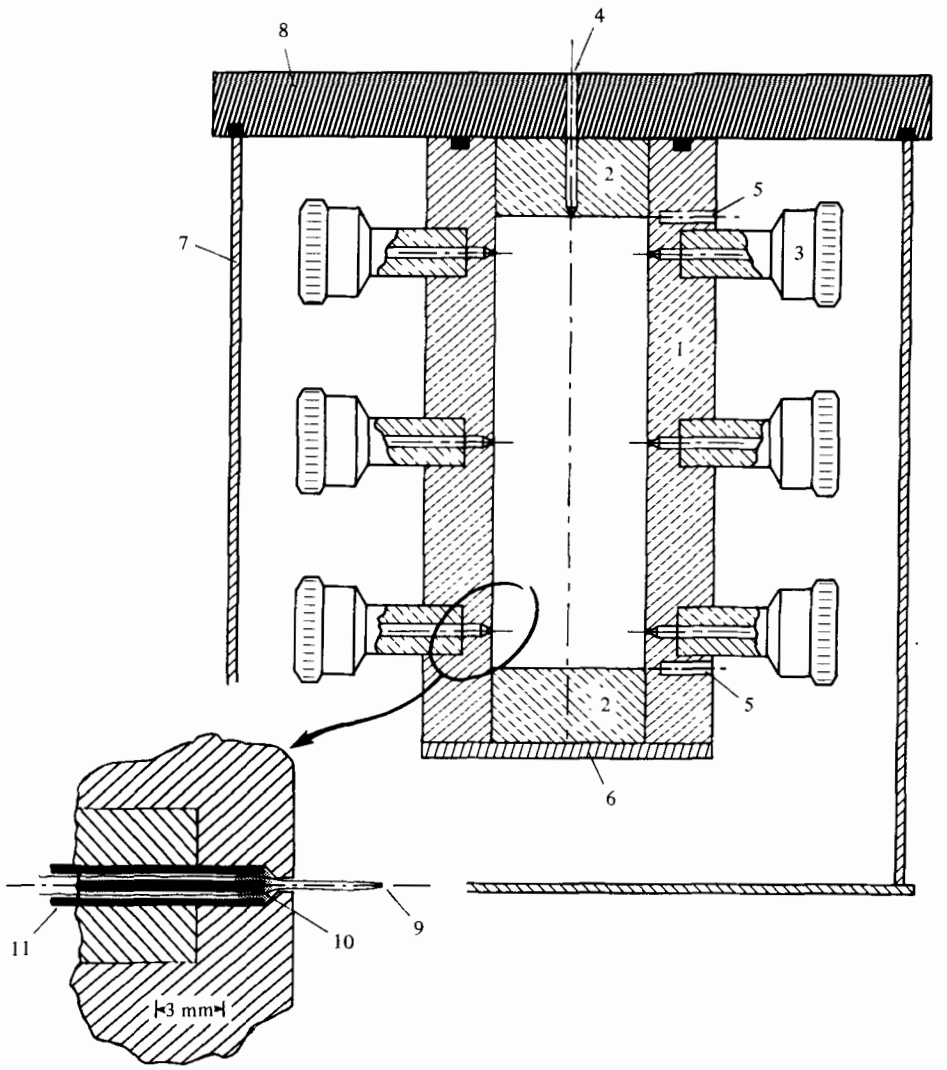

FIGURE 2. Experimental arrangement. Convection cell: (1) copper cylinder; (2) copper end plugs, press fitted; (3) o-ring feedthroughs; (4) filling port; (5) thermistor wells for $(T_h - T_c)$ measurement; (6) bottom film heater; (7) vacuum container, with (8) top plate; (9) thermistor bead; (10) Torr Seal vacuum sealant; (11) two-bore ceramic tube.

determined by a uniform film heater. The temperature of the water bath is maintained at 40 °C. With vigorous stirring and a highly sensitive temperature controller (Tronac Model 40), this water bath system is stable to $\pm 5 \times 10^{-4}$ °C. The temperature of the heater at the bottom of the cell is determined by a similar temperature controller such that the temperature difference ΔT, along the cell, is stable to $\pm 0{\cdot}05\,\%$ of ΔT.

The boundary conditions that are achieved in this experimental set-up closely approximate those used in the theoretical work of Hales (1937) and Catton (1966). The vacuum insulation effectively reduces heat losses through the side walls of the copper cell. The result is a temperature profile in the wall which deviates from a linear

distribution by less than 0·5%. Also, the ratio of the thermal conductivity of the copper walls to that of gases is approximately 10^4, which is large enough to justify the assumption that the cell walls are infinitely conducting (Ostroumov 1952).

Deviations from ideal boundary conditions undoubtedly exist. They may be due due to a slight misalignment of the cylinder axis with respect to vertical or an azimuthal variation of the heat flow from non-uniform contact between the cell and the top plate (8) and/or the bottom heater (6). Such defects are very hard to detect and control. In addition, one can show that a small, radial component of heat flux (small as compared to the axial heat flux) still exists near the ends of our convection cell. This radial heat flux exists because the constant temperature heat source and sink are located relatively far (1–2 cm) from the inner horizontal boundaries of the cell. The situation is analogous to the problem of potential flow past a step. In retrospect, the obvious solution to this problem is to move the heat source and sink as close as possible to the horizontal surfaces of the cavity, as shown in figure 1.

2.2. *Detection system*

High resolution differential thermometry was used to detect the onset of the initial and subsequent instabilities. For an illustration of the principle of the technique, consider figure 3(*a*). Owing to the convective heat transfer the unicellular, asymmetric roll establishes a temperature distribution which differs from that of the unperturbed, conductive state by the perturbation temperature T'. If the temperature sensors $R2$ and $R3$ are positioned at radially symmetric points, then

$$T'_{R2} = -T'_{R3},$$

so that the temperature difference between $R2$ and $R3$ is

$$T'_{R2} - T'_{R3} = 2T'_{R2} = -2T'_{R3} \equiv 2T'.$$

Similarly, if the planform is a 2-cell, asymmetric roll pattern (figure 3*b*), then it follows that

$$T'_{R2} - T'_{R3} = 2T' = 0. \tag{1}$$

Hence, strategically placed, sensitive differential sensor pairs can yield much qualitative and quantitative information about the convective state of the fluid, provided that the flow is asymmetric.

In order to minimize the changes in the boundary conditions from the protruding sensors we have used micro-thermistor beads 0·2 mm in diameter with 25 μm diameter Pt alloy leads. A differential pair is connected in series and forms one side of a Wheatstone bridge. The other side of the bridge is a 10 kΩ Kelvin–Varley voltage divider. The ΔT and the temperature at the midpoint of the cell, T_m are measured with thermistors imbedded in the copper wall.

This detection system has several advantages. First, with the differential technique, small fluctuations that occur simultaneously at a thermistor pair do not appear at the output of the bridge. This effectively locks out residual noise coming from, for example, imperfect temperature controllers. Secondly, thermistors are at least two orders of magnitude more sensitive than thermocouples and consequently less susceptible to problems with extraneous noise. These two properties along with the good temperature controllers used in these experiments, have allowed us to routinely

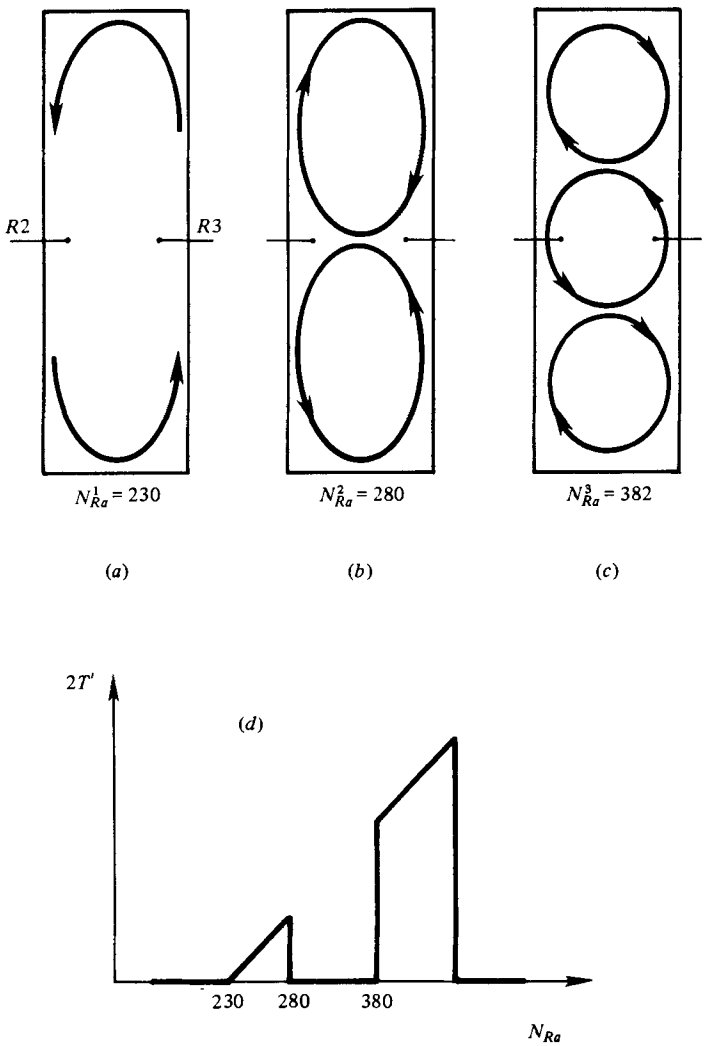

FIGURE 3. Convective flow behaviour. (*a*), (*b*) and (*c*). Schematic representations of planform for the first three modes. (*d*) Expected $2T'$ behaviour assuming that for $N_{Ra}^i \leqslant N_{Ra} < N_{Ra}^{i+1}$, only the ith mode is present.

measure temperature differences of 2×10^{-4} °C. Third, these are local measurements and hence in contrast to heat flux measurements, should be more sensitive to subtle changes in the convective flow pattern.

In any detection scheme which uses physical probes immersed in the fluid one must be concerned with the effects introduced by the probes themselves. Investigation of these effects will be discussed along with the experimental results in § 3.

2.3. *Choice of systems*

For an accurate determination of N_{Ra} the viscosity μ, thermal conductivity k, and the specific heat c_p must be known with reasonable precision. In this regard, the noble

	$\mu \times 10^6$ (g/cm s)†	$k \times 10^6$ (cal/cm s K)†	n‡	$c_p \times 10^2/R$	Reference
Kr	265·0	23·4	2·77	2·98	(Touloukian 1970)
$SiCl_4$	97·5	17·1	2·71	6·43	(Svehla 1962)
Xe	242·5	14·0	2·87	1·90	(Touloukian 1970)

† $T_1 = 313$ K.
‡ $\alpha/\mu k(T) = (\alpha/\mu k)|_{T_1} (T_1/T)^n$, $\alpha = 1/T$ for ideal gases.

TABLE 2. Transport properties and temperature dependence of $\alpha/\mu k$ for gases used in our experiments

gases are extremely well characterized (Touloukian 1970). The gases Xe and Kr were chosen for their high molecular weight so that large N_{Ra}'s could be obtained with relatively small ΔT's at a comparably low pressure. In addition the gas $SiCl_4$ was chosen for its technological importance. It has also a high molecular weight and *estimated* values of its thermophysical properties can be found in Svehla (1962).

2.4. *Procedures*

With the thermistor probes in place, the cell is first evacuated to a pressure of 10^{-2} torr and then backfilled with the desired gas. The mass density ρ of the working fluid is calculated from the ideal gas law and measurements of the filling pressure p, the temperature T and the cell volume. This density was chosen such that $\Delta T \approx 1$ °C at N_{Ra}^{cr}. The uncertainty in ρ is approximately 1 %. After the cell has been filled and sealed off, the apparatus is placed into the water bath. Thermal equilibrium is achieved within 2–3 hr.

For studies of time-independent behaviour an automatic control system is used. At intervals of 20 min this control system digitally records voltages associated with T_m, ΔT and $2T'$; and then electromechanically increases by a given amount the temperature of the bottom heater. For the small increments in ΔT used in our experiments the 20 min interval between data points was sufficient time for the experimental set-up and the convective behaviour of the gas to reach steady state.

At the end of the run the data is fed into a computer. From experimentally determined calibration tables, measured values of T_m and ΔT are adjusted for slight non-linearities in the thermistor-bridge system. For each pair $(T_m, \Delta T)$, N_{Ra} is then computed from equation

$$N_{Ra} = \left(g\rho^2 c_p a^4 \frac{\Delta T}{h}\right) \times \left.\frac{\alpha}{\mu k}\right|_{313\,\mathrm{K}} \times \left(\frac{313\,\mathrm{K}}{T_m}\right)^n. \tag{2}$$

The last term in this equation is a convenient way of expressing the temperature dependence of the quantity $\alpha/\mu k$. As the *mean* temperature of the fluid T_m changes, the *mean* thermophysical properties of the fluid [α, μ and k (see table 2)] also change. Practically, this correction amounts to about 2 % at N_{Ra}^1. The quantity n is a constant for small variations of T, and hence can be obtained from a log–log plot of $\alpha/\mu k$ *vs.* T^{-1}.

For $2T'$, more extensive manipulation is required. Below the convective threshold a plot of the measured voltages associated with $2T'$ *vs.* N_{Ra} is a straight line of non-zero slope. This is caused by a small vertical misalignment and/or a slight temperature coefficient mismatch between the two thermistors. To compensate for this effect,

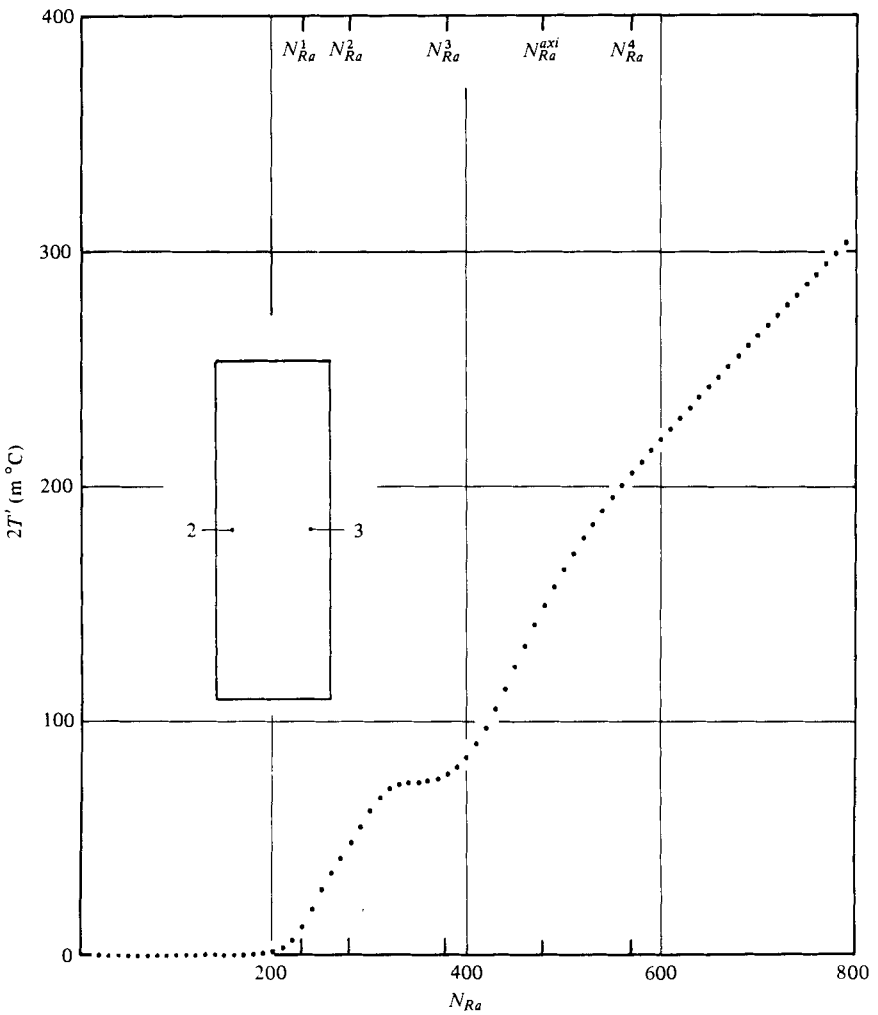

FIGURE 4. Transverse temperature difference $2T'$ between symmetric points within midplane of cell as a function of Rayleigh number N_{Ra} for xenon, $6{\cdot}03 \times 10^{-3}$ g cm^{-3}, $a = 1$ cm and $h/a = 6$. Error bars for $2T'$ are smaller than the diameter of a data point. For horizontal error bars, see text.

the straight line portion of the raw plot is extrapolated to large N_{Ra}. This line is then subtracted from the raw curve to yield the plots shown in figures 4–8.

For studies of time-dependent behaviour, fluctuations of the analog voltages associated with $2T'$ and/or T' are recorded directly on a 2-pen strip chart recorder.

3. Results and discussion

3.1. *Time-independent behaviour*

A typical plot of $2T'$ *versus* N_{Ra} is shown in figure 4. The quantity $2T'$ is the transverse temperature difference as measured by two thermistors positioned at symmetric points within the midplane of the convection cell. The immersion depth of these

thermistors is $3{\cdot}8 \pm 0{\cdot}1$ mm. The working fluid is nominally 99·9 % Xe from Matheson Gas Products. For reference we have marked in the figure the first few N^i_{Ra} predicted by Hales (1937) and Catton (1966) for a cell with thermally conducting walls and an aspect ratio of six.

The most obvious feature of figure 4 is that convective motion does set in near a value of $N_{Ra} = 230$ as predicted. The agreement is not perfect, experiment

$$(N^{\mathrm{cr}}_{Ra} = 220 \pm 12)$$

being about 5 % lower than theory. This confirms the result of Hales' (1937) analysis that the stabilizing effect of the horizontal boundaries at larger aspect ratios, i.e. $A \geqslant 6$, can be neglected. There is also a good correlation between the flat region near 380 and N^3_{Ra}. The transitions at N^2_{Ra} and N^4_{Ra} are, for these data, partially hidden for reasons that will be discussed below.

A second important result is that for $N_{Ra} \geqslant N^1_{Ra}$, $2T'$ deviates strongly from zero throughout the whole range of the experiment. Hence the flow is basically asymmetric throughout. This confirms again Hales' (1937) prediction of a (unicellular), asymmetric roll as *initial* instability; however, it disagrees with the prediction of the transition to an axisymmetric mode at $N_{Ra} = 475$. But the linear treatment can only be expected to be valid for critical and slightly supercritical flows. The nonlinear problem for large aspect ratios has not yet been solved. The experiments of Ostroumov (1952) and Slavnova (1961) in long vertical columns of water using transparent boundaries also yielded asymmetric rolls. Their experimental boundary conditions, however, deviated considerably from the theoretical boundary conditions. Lateral heat flows and nonlinear, vertical temperature profiles were undoubtedly present.

It should be pointed out that for a fixed set of experimental conditions the flow was always up one side of the cell and down the other. For a cylindrically symmetric cell and heating geometry, however, the plane of rotation of the flow pattern should be arbitrary. In other words, there are an infinite number of degenerate eigensolutions for the eigenvalue, N^1_{Ra}. The introduction of a small, asymmetric perturbation ostensibly can lift this degeneracy with the result that a preferred orientation of the roll cell becomes the dominant mode. The presence of the thermistors and/or asymmetric heat flows could be responsible for this effect.

The shape of the curve in figure 4 actually tells us much more about the modal behaviour of the convective flow. Suppose that for $N^{i+1}_{Ra} > N_{Ra} \geqslant N^i_{Ra}$, the ith mode is the only mode present. Then a plot of $|2T'|$ (for a radially symmetric thermistor pair in the midplane of the cell) *versus* N_{Ra} should resemble figure 3 (*d*). From symmetry considerations, $|2T'|$ in the midplane of the cell must go to zero for modes $i = 2$ and $i = 4$ [see figure 3*b* and equation (1)]. Comparison of figure 3 (*d*) with figure 4 shows that the above supposition is false. Hence, it appears that the general state of the fluid for a given N_{Ra} is actually a superposition of the i modes for which $N_{Ra} \geqslant N^i_{Ra}$.

We can now explain why the onset of the second and fourth modes are at least partially hidden in figure 4. For N_{Ra} slightly greater than N^2_{Ra}, the general state of the fluid is ostensibly a superposition of the first and second modes. If the second mode does not strongly couple with the first and if indeed $2T' = 0$ for the second mode, then the onset or presence of the second mode will not be detected. Careful examination

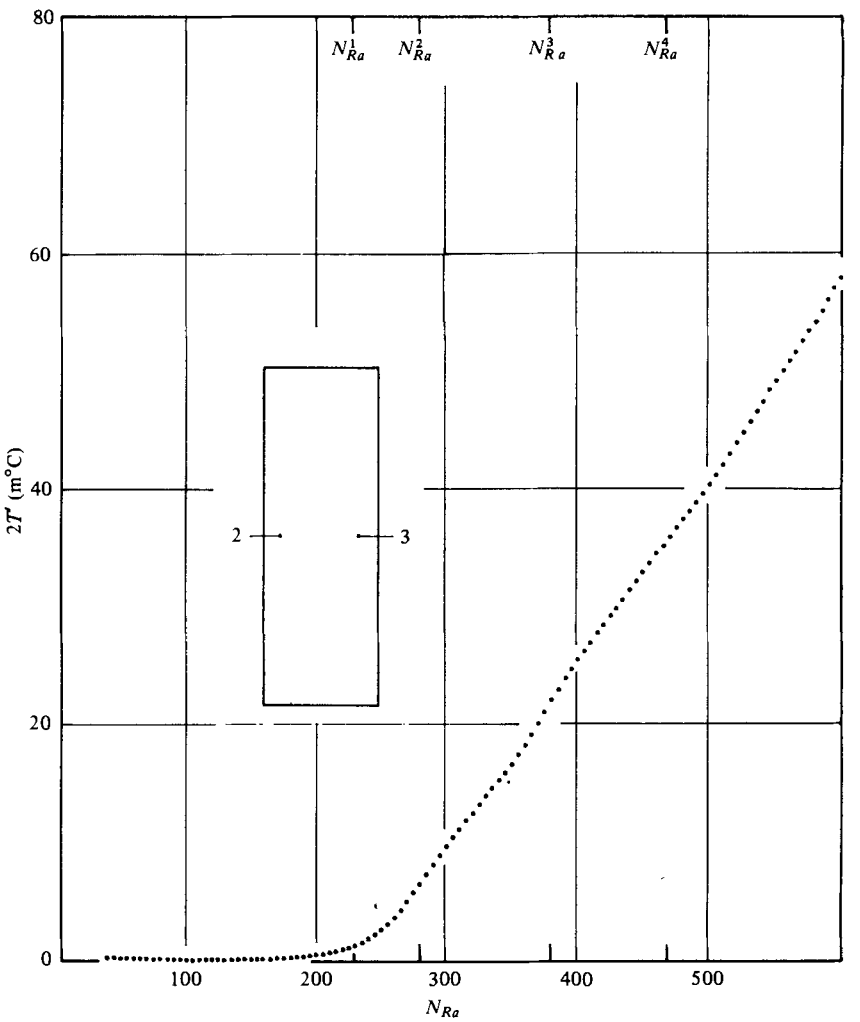

FIGURE 5. Transverse temperature difference $2T'$ in midplane *vs.* Rayleigh number N_{Ra} for $SiCl_4$ vapour, $2{\cdot}39 \times 10^{-3}$ g cm^3, a = 1 cm and h/a = 6.

of the curve near N^2_{Ra} reveals some curvature which may be attributed to the second mode, but the exact point at which the transition occurs is obscured by effects that tend to broaden the width of the transition.

Broadening effects are most evident in the first and third transitions. The transitions to the first and higher modes are seen to occur over a range ΔN_{Ra} about N^i_{Ra}. This broadening is particularly pronounced for the first and third transitions; see also figure 5 for $SiCl_4$. Graham (1973) and Smith (1974) have derived expressions for the theoretical width of the convective threshold $\Delta N_{Ra}/N^{cr}_{Ra}$ by considering the effects of hydrodynamic fluctuations. They found that for both the Bénard geometry as well as laterally confined fluids the width is approximately 10^{-7}, i.e. immeasurably small. Our experiments yield a width of approximately 10^{-1}.

Ahlers (1975), using a sensitive, probeless heat flux technique, studied the width of the transition in liquid He(N_{Pr} = 1). His first measurements yielded a width com-

parable to our findings. [As we have shown, this broadening effect will also apply to higher order transitions which could be one reason why Ahlers (1975) did not detect the discrete heat flux transitions of Malkus (1954), Willis & Deardorff (1967) and Krishnamurti (1970).] However, more recent measurements by Behringer & Ahlers (1978) using a Bénard cell constructed to closer tolerances, have yielded a transition width which is sharp within the resolution of the experimental technique. They found that small inhomogeneities in the boundaries or a non-uniform height of the convection cell were apparently responsible for the broadening effects observed initially.

In our experiment, the vertical variation of the radius is less than 0·1 % and this mechanism for broadening can probably be discounted. However broadening can also result from non-vertical heat fluxes in the walls of the cell as they may arise from a slight misalignment of the cylinder axis with respect to g or a non-uniform heat sink or source. Any horizontal component of the heat flux is sufficient to drive convection (Batchelor 1954).

To test these ideas, a series of experiments were done; a summary of the results is shown in figure 6. Curve 1 represents our best efforts for Xe. The conditions for curve 3 are identical with those for curve 1 except that the cell is tilted by 6° with respect to gravity. Curve 2 was obtained after insertion of a thin wedge of an insulating material between the copper cell and the top plate. As expected, the critical Rayleigh number N^1_{Ra} is shifted to lower values, sensitively reflecting the introduction of non-vertical heat flow. The most important result of these experiments is the marked increase in the width of the transition, especially for the non-uniform heat sink case. Hence we suspect that the junctions between the copper cell and the heat sink and source are the cause of the observed excessive broadening.

In an effort to learn more about the vertical structure of the flow pattern, four more thermistors (two differential pairs) were immersed in the fluid as shown in the insert in figure 7 (*a*) for Kr (99·9 %). The data for the three curves shown were taken simultaneously. The two thermistors in the midplane were 'on' continuously during the course of the run. The other four thermistors were only 'on' for the time that it takes to make the measurement (approximately 5 s).

For slightly supercritical values of N_{Ra}, all three curves deviate from zero in the negative direction. Though six sensors are obviously not sufficient to fully characterize the flow pattern within the cell, this finding appears to indicate that most of the cell contents convects in one asymmetric roll. A negative value of $2T'$ is indicative of clockwise rotation. At approximately $N_{Ra} = 280$ (N^2_{Ra}!), the flow in the lower two-thirds of the convection cell has reversed. This *vertically* asymmetric, 2-roll pattern, which is quite different from the vertically symmetric, multiple-roll pattern observed by Slavnova (1961), persists in its basic form well into the oscillatory regime of the convective flow.

A comparison of curve 2–3 in figure 7 (or 8) with the curve in figure 4 (or 5) reveals a significant difference. In figure 4, the transition at N^2_{Ra} is (partially) hidden, in figure 7 (*a*) it stands out. A schematic sequence of events which is consistent with this new behaviour is shown in figures 7 (*b*)–(*d*). For slightly supercritical Rayleigh numbers, the planform is a unicellular, asymmetric roll with, here, clockwise rotation (figure 7*b*). At around 280, mode $i = 2$ appears and apparently interacts with mode $i = 1$ causing it to change its direction of rotation (figure 7*c*). The superposition of mode $i = 2$ and the perturbed mode $i = 1$ gives the planform shown in figure 7*d*.

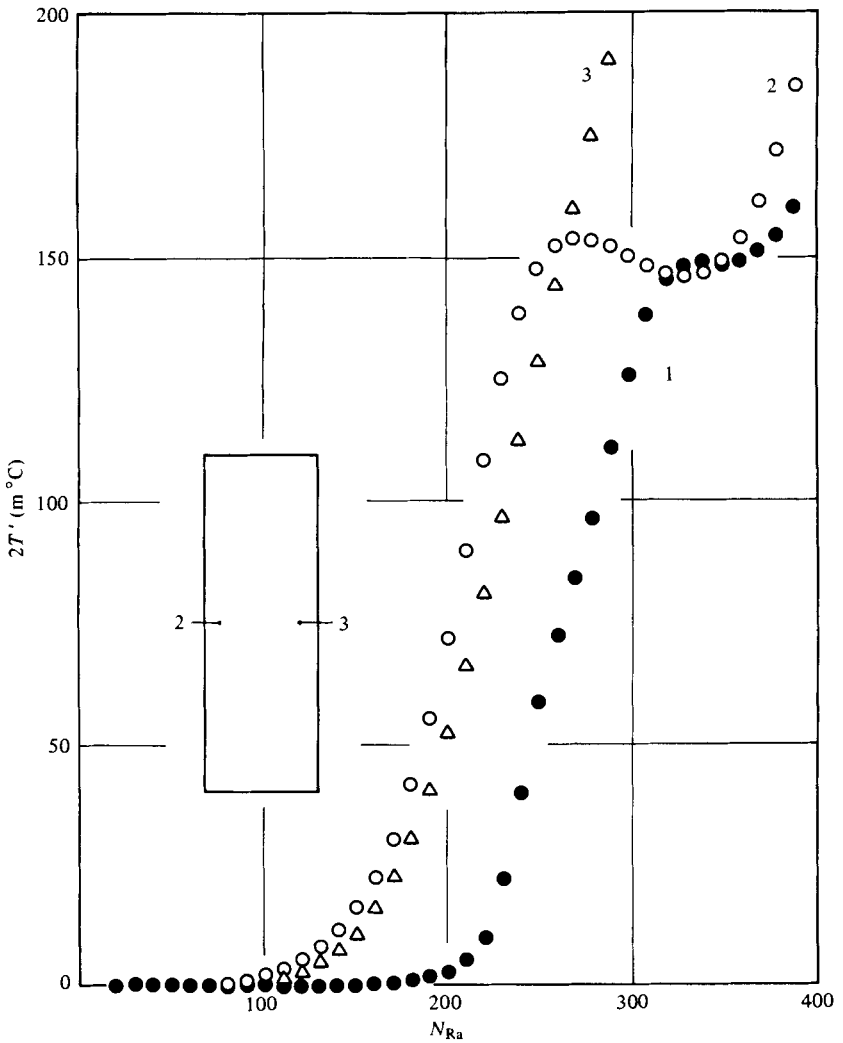

FIGURE 6. Modifications of convective behaviour of Xe by non-vertical heat flows. Data points are enlarged for graphical clarity. Vertical error bars same as for figures 4 and 5. ●, vertical symmetric heat flow; ○, asymmetric heat flow; △, tilted 6° with respect to gravity.

A similar planform has been observed by Heitz & Westwater (1971) in a square vertical column of water heated from below.

The occurrence of this new behaviour as compared to that shown in figure 4 coincides with an increase in the number of thermistor probes. There is obviously some interaction between the thermistors and the flow. We have already suggested that the presence of the thermistors may be responsible for lifting the rotational degeneracy of the roll-cell planform. However, from the results of over 20 runs using three different cells it appears that the measured N_{Ra}^{i}'s are not dependent on the number of thermistors present in the fluid. Nor are they dependent on the degree of thermistor self-heating. For example, from figure 8 it is evident that even though the thermistor self-heating was changed by one order of magnitude N_{Ra}^{cr} and N_{Ra}^{2} are virtually

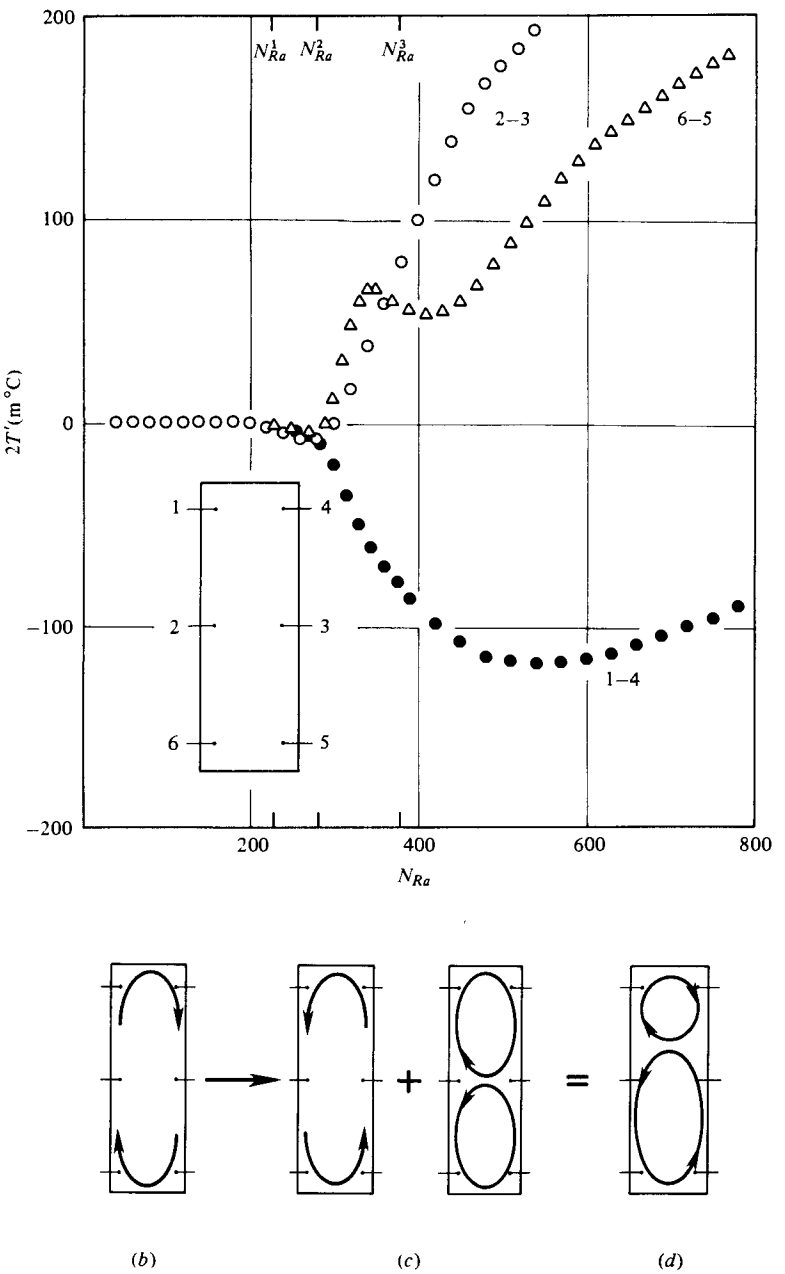

FIGURE 7. (*a*) Simultaneous measurements of $2T'$ *vs.* N_{Ra} for krypton, $6{\cdot}88 \times 10^{-3}$ g cm^{-3}, $a = 1$ cm, $h/a = 6$. (*b*), (*c*) and (*d*). Schematization of the mode–mode coupling behaviour near $N_{Ra} = 280$.

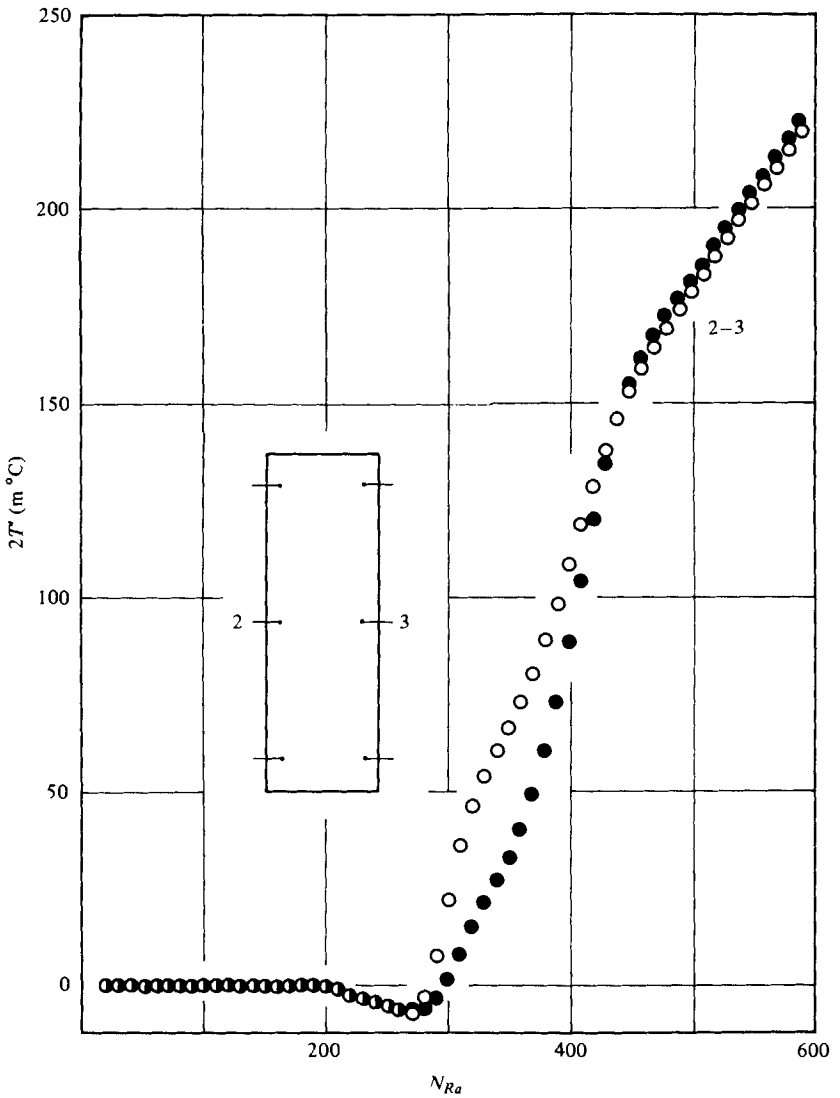

FIGURE 8. The effect of thermistor self-heating on the convective behaviour of xenon. ●, self-heating, 0·1 °C; ○, self-heating 0·01 °C.

unchanged. Our ability to detect the onset or presence of a particular convective mode may depend on the distribution (number and position) of thermistor probes, the existence or non-existence of that particular mode does not.

3.2. *Time-dependent behaviour*

There are very few studies of time-dependent convection in vertical cylinders. Mitchell & Quinn (1966) have done semiquantitative work in gaseous systems of low aspect ratio. To our knowledge the only quantitative experiments with large aspect ratio were done by Verhoeven (1969). Using liquid mercury ($N_{Pr} = 0{\cdot}025$), Verhoeven found that the critical Rayleigh number for the onset of periodic temperature fluc-

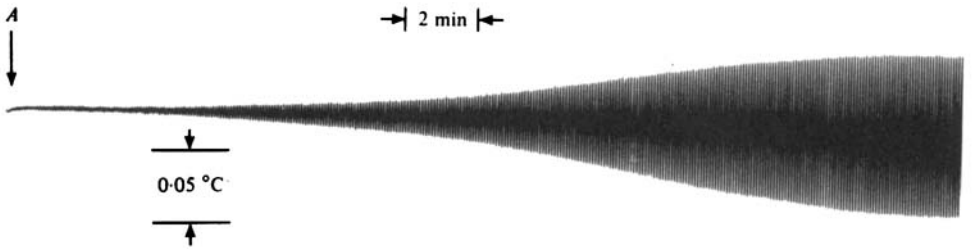

FIGURE 9. Onset of oscillations of the transverse temperature difference $2T'$ between symmetric points within the midplane of the cell for xenon. $N_{Ra} = 1321$, $\rho = 6{\cdot}03 \times 10^{-3}$ g cm^{-3}, $a = 1$ cm, $h/a = 6$.

Run	Fluid	$\rho \times 10^3$ (gm/cm^3)	N_{Ra}^{osc}
18*b*	Xe	6·00	1321
16*a*	Kr	6·88	1347
14*a*	Xe	6·00	1435
13*c*	Xe	5·69	1290

TABLE 3. Measurements of N_{Ra}^{osc}

tuations N_{Ra}^{osc} exceeded the theoretical N_{Ra}^{cr} by only 10%. This result is appropriate for low N_{Pr} fluids (liquid metals), but is of little value for the prediction of time-dependent convective behaviour of gases ($N_{Pr} \simeq 0{\cdot}7$). (Similarly the supercritical convective behaviour of gases cannot be reliably used to predict the behaviour for large Prandtl number fluids.)

Periodic temperature fluctuations. The strip chart recording in figure 9 is a typical example of the onset of oscillatory convective motion for monocomponent fluids in our experiments. Recorded are oscillations of the transverse temperature difference $2T'$ as measured by two thermistors placed at symmetric points within the midplane of the cell. Before point A in figure 9, transient temperature fluctuations with an amplitude of approximately 10^{-3} °C were present. At point A, N_{Ra} was increased by 0·5% to 1320. Within 30 min, the transient fluctuations became stable oscillations with an amplitude of approximately 0·1 °C, and a period of 5 s. Similar measurements of N_{Ra}^{osc} were made for different fillings of Xe and Kr (see table 3). The average from these runs is $N_{Ra}^{osc} = 1348$ with a standard deviation of 4%. The ratio

$$N_{Ra}^{osc}/N_{Ra}^{1} = 5{\cdot}86$$

differs significantly from data obtained from the Rayleigh–Bénard geometry using air ($N_{Pr} = 0{\cdot}7$) as the working fluid:

$$N_{Ra}^{osc}/N_{Ra}^{cr} = 3{\cdot}4 \quad \text{(Willis \& Deardorff 1970)};$$

$$N_{Ra}^{osc}/N_{Ra}^{cr} = 2{\cdot}8 \quad \text{(Krishnamurti 1970)}.$$

Previous to this work it was suspected that N_{Ra}^{osc}/N_{Ra}^{cr} might be independent of the aspect ratio. From these results there is little doubt that it is not. The close proximity of the vertical walls has a greater stabilizing effect near the point where oscillatory phenomena set in than at the point of marginal instability, N_{Ra}^{cr}.

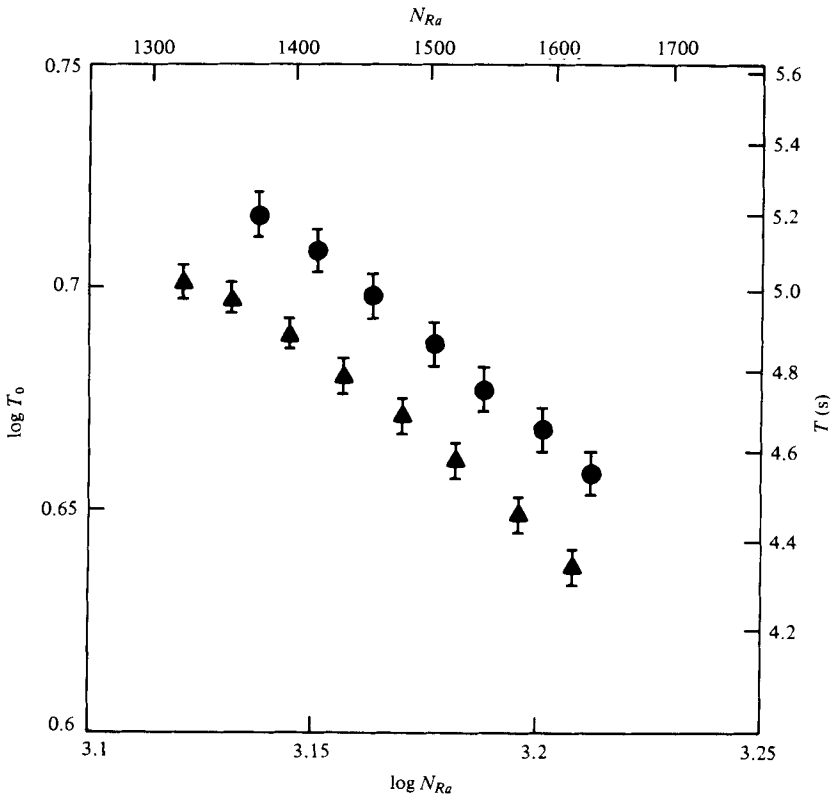

FIGURE 10. Period T_0 of oscillations of the transverse temperature difference $2T'$ *vs.* N_{Ra} for: ▲, Xe, $6{\cdot}03 \times 10^{-3}$ g cm^{-3}; ●, Kr, $6{\cdot}88 \times 10^{-3}$ g cm^{-3}.

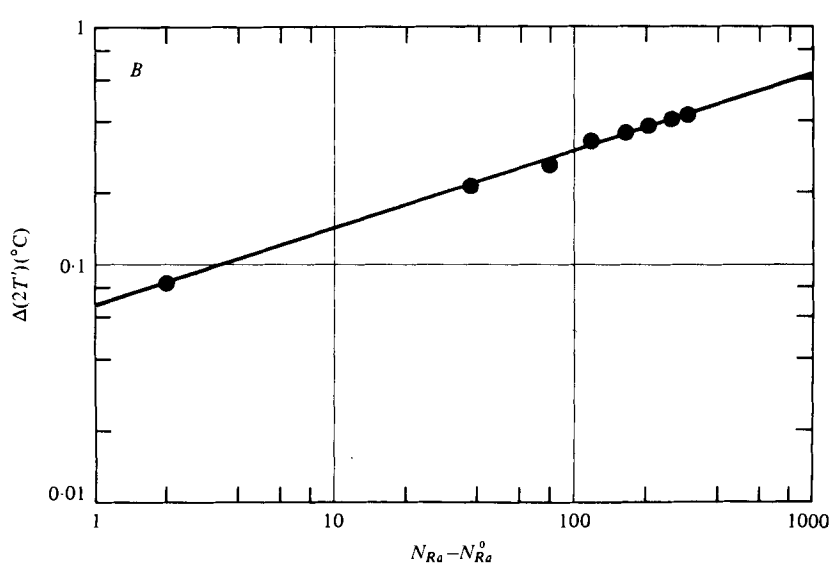

FIGURE 11. Peak-to-peak amplitude of transverse temperature difference oscillations $\Delta(2T')$ *vs.* N_{Ra} for Xe, $\rho = 6{\cdot}03 \times 10^{-3}$ g cm^{-3}, $N_{Ra} = 1318$.

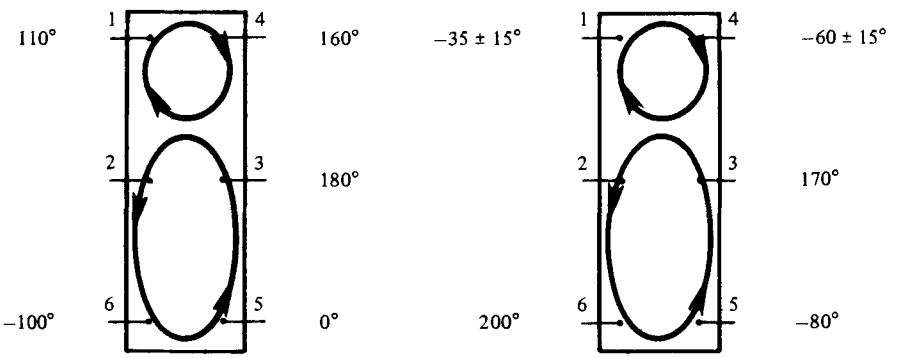

FIGURE 12. Phase angle (relative to $R2$) of temperature oscillations in various parts of the cell for Xe, $\rho = 6{\cdot}03 \times 10^3$ g cm^{-3}, (*a*) $N_{Ra} = 1321$. (*b*) $N_{Ra} = 1538$.

The oscillation results obtained for Xe (e.g. figure 9) and the other monocomponent gases used in this study can be summarized as follows.

(1) With $T_0 = 5$ s, the period of the oscillations is relatively short.

(2) The amplitude of the oscillations $\Delta 2T'$ relative to the time-independent magnitude of $2T'$ at N_{Ra}^{osc} is approximately

$$\Delta 2T'/2T' = 0{\cdot}1\ ^\circ\text{C}/0{\cdot}6\ ^\circ\text{C} = \tfrac{1}{6}.$$

(3) The oscillations are symmetric about the time axis that passes through point A corresponding to the time-independent $2T'$. Combined with the previous result, it is then apparent that the oscillations are symmetric disturbances of the mean flow.

(4) As N_{Ra} is increased above N_{Ra}^{osc}, (*a*) the period T_0 of the oscillations decreases with increasing N_{Ra} (see figure 10); (*b*) the amplitude of the oscillations $\Delta(2T')$ increases with increasing N_{Ra} (see figure 11).

For the Rayleigh–Bénard geometry the functional relationship between T_0 and N_{Ra} can be used as a guide for determining the mechanism which generates the temperature oscillations (Carruthers 1976). As far as we can discern, however, none of the mechanisms proposed so far can account for the results shown in figure 10 or the complex phase structure shown in figure 12. In this respect the data shown in figure 11 is also without precedence and as yet remains unexplained.

If one deviates significantly from the conditions as described at the beginning of this paper, the characteristics of the oscillations change drastically. The most important example is the subject of the next paper, which describes the convective behaviour of two-component gases (Olson & Rosenberger 1979).

Transition to aperiodic behaviour. As mentioned in the previous section, the oscillatory behaviour of the fluid flow is, in most cases, a simple well-behaved function of N_{Ra}. However, for increasing values of $N_{Ra} > N_{Ra}^{\text{osc}}$, a sequence of events occurs which contributes to the eventual decay of periodic behaviour near $N_{Ra} = 1700$. Basic features of this transition region can be summarized as follows.

For N_{Ra} about 10% greater than N_{Ra}^{osc}, the oscillatory temperature fluctuations in the various parts of the cell are virtually sinusoidal with the same fundamental frequency ω_0 (but not the same amplitude); see figure 13(*a*).

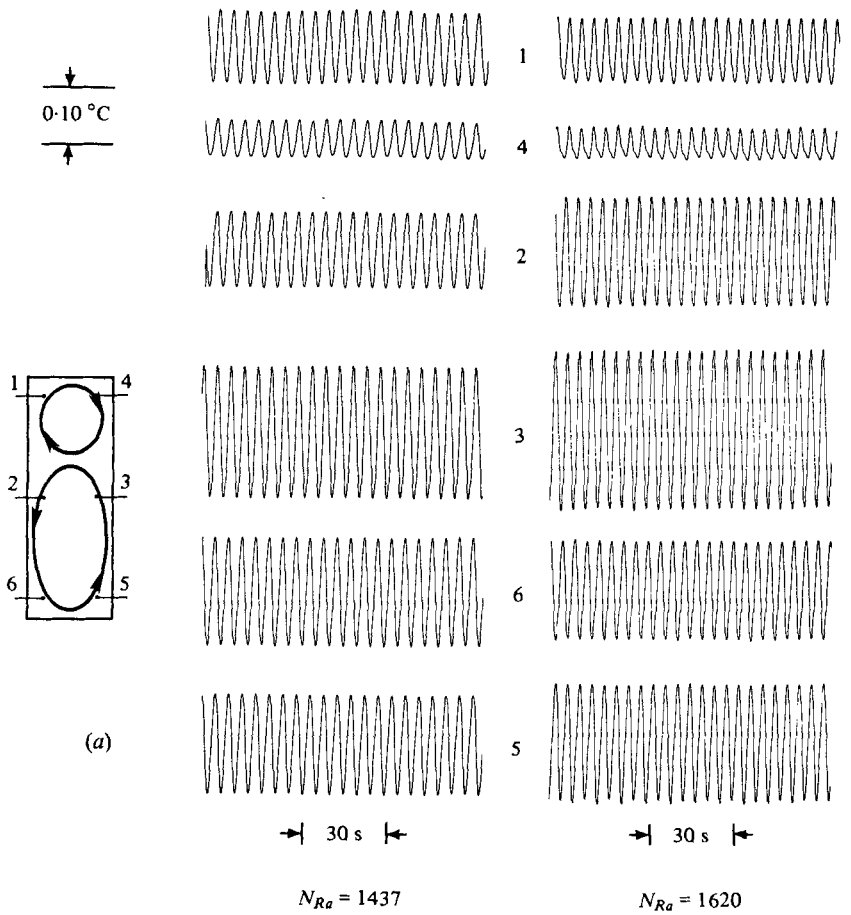

FIGURE 13 (*a*). For legend see facing page.

At $N_{Ra} = 1620$ (figure 13*a*), evidence for the onset of a second oscillatory mode with frequency $\frac{1}{2}\omega_0$ can be seen as distortions of the sinusoidal waveforms. This is especially evident in the waveform measured by $R4$, a *corner* thermistor. The mechanism for generating this second mode is not known at this time, but boundary layer separation and subsequent vortex formation are possible mechanisms.

At $N_{Ra} \simeq 1670$ (figure 13*b*), temperature fluctuations at the other five thermistors ($R1$, $R2$, $R3$, $R5$ and $R6$) now reflect the presence of the second mode. A third mode with frequency $\frac{1}{4}\omega_0$ has now been added to the spectrum at $R4$, and superimposed upon all six spectra is a low frequency oscillation with $\omega \simeq \frac{1}{12}\omega_0$. This low frequency oscillation is more easily seen in the time-contracted version below the waveform for $R5$.

At $N_{Ra} \simeq 1700$, waveforms which are essentially aperiodic are now present at all six thermistors. Note, however, that the fluctuations at $R1$ and $R4$ and at $R2$ and $R3$ are still spatially correlated. Looking back we can clearly discern already at $N_{Ra} = 1620$ features which eventually lead to the aperiodic behaviour at $N_{Ra} \simeq 1700$.

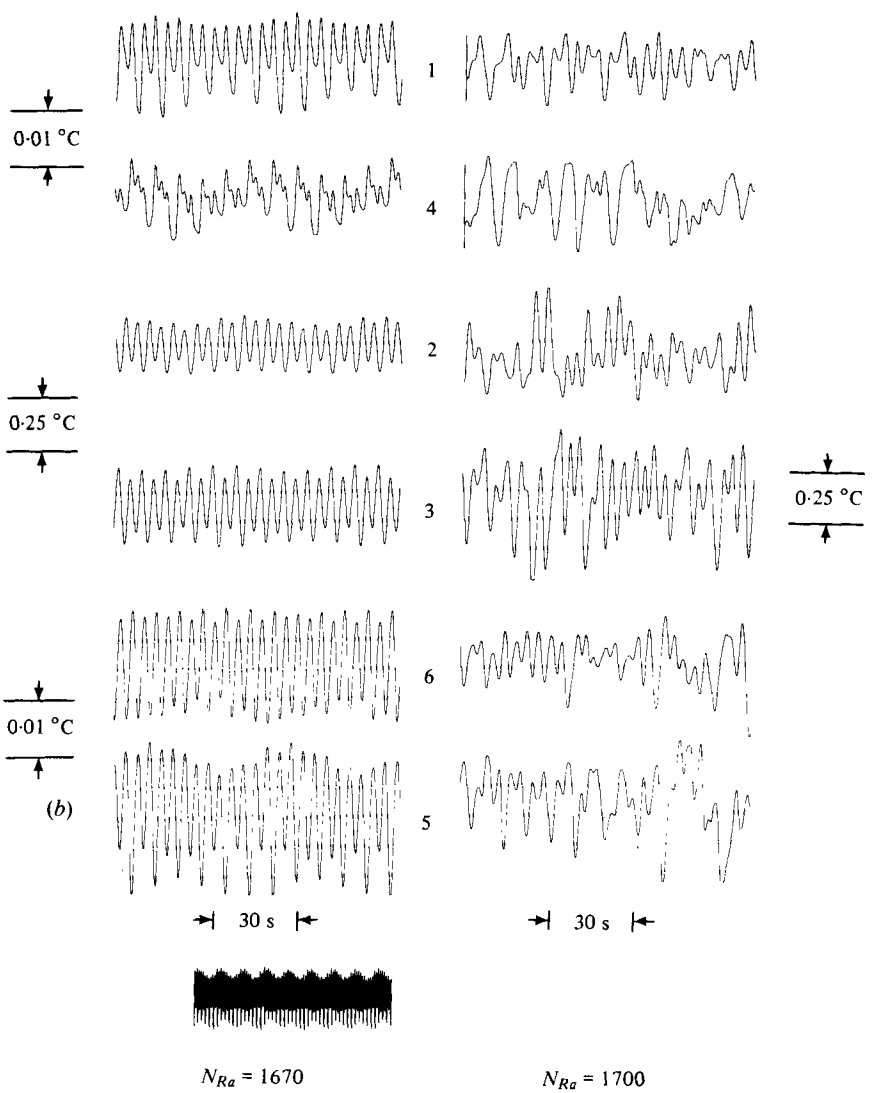

FIGURE 13. (*a*, *b*) Transition to aperiodic behaviour. The traces represent the absolute temperature variations at the location of the individual thermistors, in contrast to the differential measurements depicted in the earlier figures.

4. Summary and conclusions

We have presented and discussed the results of experiments designed to study the stability of a column of fluid heated from below. Broad yet distinctive features (changes in slope) in plots of transverse temperature differences *vs.* N_{Ra} correlate quite well with the N_{Ra}^{i} taken from the theoretical work of Hales (1937) and Catton (1966). The planform of the convective flow is basically asymmetric, even above $N_{Ra} = 475$ where the first axisymmetric mode can become stable (Hales 1937). In addition, evidence was presented which supports the contention that the general,

time-independent state of the fluid for a given N_{Ra} is actually a superposition of the i modes for which $N_{Ra} \geqslant N_{Ra}^{i}$.

New and important results were also obtained for the time-dependent behaviour of the fluid. The value of N_{Ra}^{osc}/N_{Ra}^{cr} for the fully confined geometry investigated here is quite different from the results for the Rayleigh–Bénard geometry.

In general, it was found that the convective behaviour of a *column* of fluid heated from below bears little resemblance to that of a fluid *layer* heated from below (Rayleigh-Bénard problem). This lack of similarity has diminished the chances of transferring the vast body of literature which surrounds the Rayleigh–Bénard problem to the problem studied here. Finally it underscores the vital need for more work on fully confined fluids.

This work was supported by the National Science Foundation under grant number DMR75-03175; and by research grants from the Crystal Products Department, Union Carbide Corporation, and the Electronics Materials Committee of AIME. We also thank Mr M. Ivarsson for the skilful machine work and Mr E. L. Kimber for extensive electronics advice.

REFERENCES

AHLERS, G. 1975 The Rayleigh–Bénard instability at helium temperatures. In *Fluctuations, Instabilities and Phase Transitions* (ed. T. Riste). New York: Plenum.

BATCHELOR, G. K. 1954 Heat transfer by free convection across a closed cavity between vertical boundaries at different temperatures. *Quart. Appl. Math.* **12**, 209.

BEHRINGER, R. & AHLERS, G. 1978 Evolution of turbulence form the Rayleigh–Bénard instability. *Phys. Rev. Lett.* **40**, 712.

CARRUTHERS, J. R. 1976 Origins of convective temperature oscillations in crystal growth melts. *J. Cryst. Growth* **32**, 13.

CATTON, I. 1966 The effect of lateral boundaries on natural convection between horizontal surfaces. Ph.D. dissertation, UCLA.

CHARLSON, G. S. & SANI, R. L. 1971 On thermoconvective instability in a bounded cylindrical fluid layer. *Int. J. Heat Mass Transfer* **14**, 2157.

GRAHAM, R. 1973 Generalized thermodynamic potential for the convection instability. *Phys. Rev. Lett.* **31**, 1479.

HALES, A. L. 1937 Convection currents in geysers. *Roy. Astro. Soc. Geophys. Suppl.* **4**, 122.

HEITZ, W. L. & WESTWATER, J. W. 1971 Critical Rayleigh numbers for natural convection of water confined in square cells with L/D from 0·5 to 8. *Trans. A.S.M.E. J. Heat Transfer* **93**, 188.

KOSCHMIEDER, E. L. 1974 Bénard convection. *Adv. Chem. Phys.* **26**, 177.

KRISHNAMURTI, R. 1970 On the transition to turbulent convection. Part 2. The transition to time-dependent flow. *J. Fluid Mech.* **42**, 309.

MALKUS, W. V. R. 1954 Discrete transitions in turbulent convection. *Proc. Roy. Soc.* A **225**, 185.

MITCHELL, W. T. & QUINN, J. A. 1966 Thermal convection in a completely confined fluid layer. *A.I.Ch.E. J.* **12**, 1116.

OLSON, J. M. & ROSENBERGER, F. 1979 Convective instabilities in a closed vertical cylinder. Part 2. Binary gas mixtures. *J. Fluid Mech.* **92**, 631–642.

OSTROUMOV, G. A. 1952 Free convection under the conditions of the internal problems. *Tech. Theor. Lit.* Moscow–Leningrad: State Publishing House. [Engl. trans. *N.A.C.A.*-TM-1407 (1958).]

SLAVNOVA, E. I. 1961 On the cellular structure of the convective flow of a fluid in a vertical cylinder of circular cross section. *Inzh. Fiz. Zh.* **4**, 80.

SMITH, W. A. 1974 Temporal correlations near the convective-instability threshold. *Phys. Rev. Lett.* **32**, 1164.

SVEHLA, R. A. 1962 Estimated viscosities and thermal conductivities of gases at high temperatures. *N.A.S.A. Tech. Rep.* R-132.

TOULOUKIAN, Y. S. 1970 *Thermophysical Properties of Matter*. New York: Plenum.

VERHOEVEN, J. D. 1969 Experimental study of thermal convection in a vertical cylinder of mercury heated from below. *Phys. Fluids* **12**, 1733.

WHITEHEAD, J. A. 1975 A Survey of Hydrodynamic Instabilities. In *Fluctuations, Instabilities, and Phase Transitions* (ed. T. Riste). New York: Plenum.

WILLIS, G. E. & DEARDORFF, J. W. 1967 Confirmation and renumbering of the discrete heat flux transitions of Malkus. *Phys. Fluids* **10**, 1861.

WILLIS, G. E. & DEARDORFF, J. W. 1970 The oscillatory motions of Rayleigh convection. *J. Fluid Mech.* **44**, 661.

YIH, C. S. 1959 Thermal instability of viscous fluids. *Quart. Appl. Math.* **17**, 25.